Journal of Crystal Growth 340 (2012) 28–33

Contents lists available at SciVerse ScienceDirect

Journal of Crystal Growth

journal homepage: www.elsevier.com/locate/jcrysgro

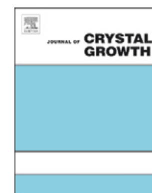

A systematic study of the nitridation of SnO_2 nanowires grown by the vapor liquid solid mechanism

Matthew Zervos [a,*], Andreas Othonos [b]

[a] Nanostructured Materials and Devices Laboratory, Department of Mechanical Engineering, Materials Science Group, School of Engineering, University of Cyprus, PO Box 20537, Nicosia 1678, Cyprus

[b] Research Centre of Ultrafast Science, Department of Physics, University of Cyprus, PO Box 20537, Nicosia, Cyprus

ARTICLE INFO

Article history:
Received 6 June 2011
Received in revised form
21 November 2011
Accepted 24 November 2011
Communicated by K. Deppert
Available online 9 December 2011

Keywords:
B1. Oxides
B1. Nitrides
A1. Nanostructures
B1. Nanomaterials

ABSTRACT

SnO_2 nanowires (NWs) with diameters of 50 nm and lengths $\geq 10\ \mu m$ have been grown at 800 °C on 1.0 nm Au/Si(001) via the vapor liquid solid mechanism and the low pressure chemical vapor deposition. These exhibited clear peaks in the X-ray diffraction corresponding to the tetragonal rutile crystal structure of SnO_2 and a broad-symmetric photoluminescence (PL) spectrum, centered around 560 nm due to structural-related defect states, energetically located in the upper half-band-gap of SnO_2. We find that post-growth thermal annealing of the SnO_2 NWs over a broad range of temperatures, i.e. 400–1000 °C and high flow of O_2 does not change their crystal structure or optical properties. In contrast the nitridation of SnO_2 NWs using NH_3 leads to their elimination above 500 °C. Lower temperatures did not favor the nitridation even using extended nitridation times, hydrogen, lower ramp rates or a two-step-temperature process which are effective in the case of In_2O_3 and Ga_2O_3. However the nitridation of SnO_2 NWs was promoted by HCl, supplied in-situ via the sublimation of NH_4Cl, which reacts with Sn and SnO_2 leading to the formation of the intermediate $SnCl_4$, which reacts in turn with NH_3 giving tin nitride at temperatures between 400 and 500 °C . We discuss the effect of the nitridation and thermal annealing on the PL spectra.

© 2011 Elsevier B.V. All rights reserved.

1. Introduction

Group III-Nitride (III-N) semiconductor nanowires (NWs) such as InN [1], GaN [2] and InGaN [3] have recently attracted considerable attention for the fabrication of high efficiency solar cells since they can absorb photons across the full spectrum in contrast to their -As or -P counterparts. Nevertheless a significant drawback of the Group III-Nitrides is their high cost so viable alternatives are required in order to provide a cost–benefit advantage.

Group IV-Nitride (IV-N) semiconductors on the other hand, such as Si_3N_4 [4] and Ge_3N_4 [5] have been investigated mainly as dielectrics, but Sn_3N_4, which has been proposed as a material for energy storage [6] and solar cells [7], has not been investigated despite the fact that Sn has a low melting point of 232 °C and is cheap. To date Sn_3N_4 films have been grown by halide chemical vapor deposition [8,9], metal organic chemical vapor deposition (MOCVD) [10], sputtering [11–14] and ammonothermal synthesis [15,16]. However there are very few investigations on Sn_3N_4 nanowires (NWs), which could be used as nanostructured materials for the fabrication of third generation solar cells. To be exact tin nitride nanoparticles (NPs) have been obtained by Nand et al. [17] while recently we obtained for the first time Sn-rich tin nitride NWs with diameters of 100 nm and lengths of a few micrometers [18,19,26] by halide CVD. In addition we have grown and investigated the optical properties of metal oxide (MO) nanowires, i.e. SnO_2, In_2O_3 and β-Ga_2O_3 [20–22] NWs and their conversion into nitrides via post-growth nitridation using NH_3 and H_2 [23,24]. We found that it is possible to obtain InN and GaN NWs via the post-growth nitridation of In_2O_3 and Ga_2O_3 NWs, respectively, so here we have undertaken a systematic investigation into the nitridation of SnO_2 NWs in order to improve our understanding of Sn_3N_4 and enable further investigations on its potential as a material for solar cell devices.

Such an investigation has not been carried out previously despite the fact that Sn is cheap with a low melting point and SnO_2 NWs have been grown and studied extensively in the past. Here it should be pointed out that MO NWs such as SnO_2 can be grown easily with diameters of a few tens of nanometers, lengths of tens of micrometers and a high yield and uniformity in contrast to their nitride counterparts, which are considerably more difficult to obtain and control.

Therefore we have grown SnO_2 NWs with diameters of 50 nm's and lengths $>10\ \mu m$ by low pressure chemical vapor deposition

* Corresponding author. Tel.: +357 228 94 509; fax: +357 228 92 254.
E-mail address: zervos@ucy.ac.cy (M. Zervos).

0022-0248/$ - see front matter © 2011 Elsevier B.V. All rights reserved.
doi:10.1016/j.jcrysgro.2011.11.063

(LPCVD) and find that the post-growth thermal annealing of the SnO_2 NWs between 400 and 1000 °C under O_2 does not change their crystal structure or optical properties. In contrast the nitridation of SnO_2 NWs using NH_3 leads to their elimination at temperatures > 500 °C. Lower temperatures did not favor the formation of tin nitride even after extended nitridation times or using hydrogen, lower ramp rates or by employing two-step temperature nitridations. It is found that the post-growth nitridation of SnO_2 NWs is promoted for temperatures in the range 400–500 °C by HCl, supplied in-situ via the sublimation of NH_4Cl, which reacts with Sn and SnO_2 leading to the formation of $SnCl_4$ and its subsequent reaction with NH_3 giving tin nitride. More importantly we find that the integrity of the SnO_2 NWs is maintained, which is important for the fabrication of devices but the PL does not change significantly by post-growth thermal annealing or nitridation.

2. Experimental method

Initially SnO_2 NWs were grown using an LPCVD reactor consisting of four mass flow controllers and a 1 in. horizontal quartz tube (QT) furnace capable of reaching 1100 °C and a base pressure of 10^{-4} mBar using a chemically resistant, two stage, rotary vane pump with a pumping capacity of 15 m^3/h, connected downstream. The pressure inside the 1 in. QT was adjusted manually during growth via a micro-flow leak valve connected after the mass flow controller manifold on the upstream side of the 1 in. QT. In addition the pressure gage (PG) was connected upstream after the micro-flow leak valve to prevent its contamination from Sn.

For the growth of SnO_2 NWs, 0.2 g of fine Sn powder (Aldrich, Mesh-100, 99.99%) was weighed and loaded in a quartz boat while square pieces of n^+ Si(001) ≈ 7 mm × 7 mm, coated with ≈ 1.0 nm of Au, were loaded ≈ 10 mm away from the Sn. The Au was deposited by sputtering on n^+ Si(001) after cleaning the latter in trichloroethylene, methanol, acetone and isopropanol, rinsing in de-ionized water and removing the native oxide in HF. The boat was positioned directly above the thermocouple used to measure the heater temperature at the center of the 1 in. QT. After loading, the 1 in. QT was pumped down to 10^{-4} mBar and then an Ar:2% O_2 mixture was introduced at RT for 10 min. Following this the temperature was ramped to 800 °C using Ar:2% O_2 at a rate of 30 °C/min. Upon reaching the growth temperature (T_G), the same flow of Ar:2% O_2 was maintained at 10^{-1} mBar for a further 60 min in order to grow the SnO_2 NWs after which the reactor was allowed to cool down slowly for at least 30 min. The sample was always removed when the temperature was lower than 100 °C after bringing the 1 in. QT up to 10^3 mBar, i.e. 1 atm using Ar.

The post-growth thermal annealing of the SnO_2 NWs was carried out at 10^3 mBar in a new 1 in. QT without any solid precursors. After loading each sample with SnO_2 NWs from the downstream side, a flow of 500 sccm O_2 was set for 5 min after which the temperature was ramped to the post-growth annealing temperature (T_A) under a flow of 100 sccm O_2 using a ramp rate of 30 °C/min. Upon reaching T_A, the flow O_2 was increased to 1000 sccm for 1 h after which the reactor was allowed to cool down to RT over 30 min under a reduced flow of 100 sccm O_2. A list of the different temperatures used for the thermal annealing of the SnO_2 NWs are shown in Table 1.

Similarly nitridations were carried out using NH_3. After flushing the 1″QT with 500 sccm of Ar for 10 min, the temperature was ramped to T_N under a flow of 200 sccm of NH_3 using a ramp rate of 30 °C/min. Upon reaching T_N, the same flow of NH_3 was maintained for 1 h after which the reactor was allowed to cool down to RT under a flow of NH_3. Nitridations were also carried out using H_2:NH_3, in which case the % H_2 content was varied while maintaining a total flow of 200 sccm. All other nitridation conditions were kept equal as described above. In addition a two-step nitridation process was carried out using 160 sccm of NH_3 and 40 sccm H_2 as listed in Table 1, in which case only the second ramp rate was smaller. Finally nitridations were also carried out at different temperatures using anhydrous NH_4Cl (99% VWR) and/or Sn, which were loaded ≈ 10 mm away from the SnO_2 NWs. In this case the reactor was flushed for 10 min with 500 sccm of Ar and the temperature was ramped to the desired nitridation temperature T_N using a slow ramp rate of 10 °C/min under a flow of 250 sccm of NH_3. Upon reaching T_N the same flow of NH_3 was maintained for a further 60 min. Details of the relevant growth conditions are listed in Table 2.

The morphology of the SnO_2 NWs was examined with a TESCAN scanning electron microscope (SEM) while their crystal

Table 1
Summary of post-growth oxidation and nitridation conditions for the SnO_2 NWs. In the case of post-growth oxidation the temperature was increased up to T_{OX} under a flow of 100 sccm O_2 after which the SnO_2 NWs were subjected to 1000 sccm of O_2 for 60 min . For the nitridations the 1 in. QT was flushed with 500 sccm of Ar at RT and then the temperature was ramped to T_N at 30 °C/min under 200 sccm NH_3 after which the temperature was held fixed for 60 min before cooling down. Nitridations were also carried out using NH_3: H_2 as opposed to NH_3 only, in which case the H_2% content was varied in a systematic way as shown above, while maintaining a total flow of 200 sccm, keeping everything else equal. Finally in the case of the two step temperature nitridation process 160 sccm of NH_3 and 40 sccm H_2 were used but the second ramp rate was slower than 30 °C/min used during the first ramp. The duration of both steps was equal to 60 min.

T_{OX} (°C) Oxidation		T_N (°C) Nitridation		
CVD465	400	CVD901	400	1 h
CVD464	500	CVD902	500	1 h
CVD461	600	CVD904	510	1 h
CVD459	700	CVD903	520	1 h
CVD460	800	CVD906	530	1 h
CVD462	900	CVD907	550	1 h
CVD463	1000	CVD908	600	1 h
		Nitridation–Hydrogenation		
		CVD901	400	0%H_2
		CVD893	400	10%H_2
		CVD891	400	20%H_2
		CVD897	400	30%H_2
		CVD898	400	40%H_2
		CVD899	400	50%H_2
		Two-step nitridation process		
		CVD895	400/500	10 °C/min
		CVD900	400/550	5 °C/min
		CVD896	400/600	5 °C/min

Table 2
Summary of post-growth nitridation conditions of the SnO_2 NWs using 1 g of NH_4Cl only, left-panel, or 0.1 g Sn:0.1 g NH_4Cl, right-panel. In this case the temperature was ramped to T_N using a slow ramp rate of 10 °C/min after which the temperature was held fixed for 60 min before cooling down using a flow of 250 sccm NH_3 throughout.

NH_4Cl	T_N (°C)	NH_4Cl:Sn	T_N (°C)
CVD910	325	CVD916	360
CVD912	350	CVD960	400
CVD913	360	CVD918	425
CVD911	375	CVD958	450
CVD909	425	CVD959	475
–	–	CVD919	500

structure and phase purity were investigated using a SHIMADZU, XRD-6000, X-ray diffractometer with Cu-Ka source, by performing a scan of θ–2θ in the range between 10° and 80°. In addition the morphology and XRD of the SnO_2 NWs was also investigated after thermal annealing and nitridation in order to find out if distortions occurred and determine the changes in crystal structure. Lastly the photoluminescence (PL) of the SnO_2 NWs and those treated under O_2, NH_3:H_2 and Sn:NH_4Cl were also measured between 77 and 300 K using an excitation of λ=267 nm. The pulse excitation was generated by frequency doubling the beam from an *Optical Parametric Amplifier* (OPA) using BBO second harmonic crystal. The OPA was pumped by the beam generated from with a mode-locked Ti:Sapphire laser. The pulses in the UV were 100 fs FWHM at a repetition rate of 250 kHz. The energy per pulse incident on the samples was 40 pJ over a spot of 2 mm in diameter.

3. Results and discussion

In contrast to InN NWs [1] and GaN NWs [2], we found previously, that Sn_3N_4 NWs cannot be obtained by the direct nitridation of Sn with NH_3, which lead to the preferential formation of Sn droplets over a wide range of temperatures and gas flows. A high-yield uniform distribution of tin nitride NWs with diameters of 100 nm and lengths of a few micrometers was obtained only via the formation of the halides $SnCl_2$ or $SnCl_4$, which react readily with NH_3 [18,19]. Now as stated above MO NWs such as In_2O_3, β-Ga_2O_3 and SnO_2 [20–22] can be grown easily with diameters of a few tens of nanometers, lengths of tens of micrometers and a high yield and uniformity in contrast to their nitride counterparts, which are considerably more difficult to obtain by comparison. Moreover we have obtained InN and GaN NWs via the post-growth nitridation of In_2O_3 and Ga_2O_3 NWs [23,24] so we will begin by considering the growth and properties of the SnO_2 NWs and then their nitridation.

SnO_2 NWs with diameters of 50 nm were obtained previously at 700 °C by atmospheric pressure chemical vapor deposition (APCVD) under a flow of pure Ar via the reaction of Sn with residual O_2 [20]. A high yield of SnO_2 NWs was obtained but their lengths did not exceed a few micrometers due to the limited vapor pressure of Sn over the Au/Si(001) as a consequence of the reaction of the Sn source located upstream with O_2 and the formation of a vapor limiting shell. No SnO_2 NWs were obtained under a flow of a few tens of sccm of O_2 by APCVD.

Here we have obtained a very high yield, uniform distribution of SnO_2 NWs by LPCVD at 10^{-1} mBar using Ar:2%O_2. A typical image of SnO_2 NWs that were obtained at T_G=800 °C is shown in Fig.1. The high yield-uniform distribution extending over 1 cm^2 was obtained due to the enhanced vapor pressure of Sn at 10^{-1} mBar, which led to a dense white like deposit of SnO_2 NWs with diameters of ≈50 nm and lengths of several tens of micrometers. No SnO_2 NWs were obtained on plain Si(001). This is clearly shown in the inset of Fig.1 where SnO_2 NWs were grown on 100μm × 100 μm Au squares defined on Si(001) by electron beam lithography (EBL). The existence of Au NPs on the ends of the SnO_2 NWs shown in Fig.1 suggest that they grow via a vapor liquid solid (VLS) like mechanism. However it appears that there is no epitaxial relation between individual SnO_2 NWs and the n^+ Si(001) since we observed a lateral type of network of SnO_2 NWs on the n^+ Si(001) surface after harvesting the SnO_2 NWs in isopropanol under ultrasonic vibration. In other words one dimensional growth proceeds via a particle mediated mechanism following the formation of a lateral network of SnO_2 NWs on the Au/n^+Si(001) surface during the initial stages of growth from which SnO_2 NWs grow vertically upwards thereafter.

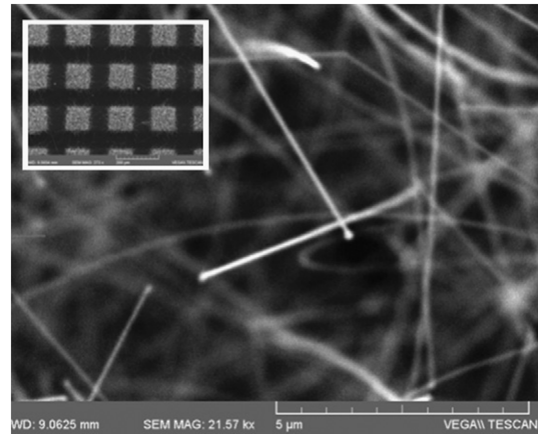

Fig. 1. Typical SEM image of SnO_2 NWs grown by LPCVD at 800 °C on 1 nm Au/Si(001). One may observe Au NPs on their ends while the inset shows SnO_2 NWs obtained on 100 μm × 100 μm Au squares, fabricated on Si(001) by EBL.

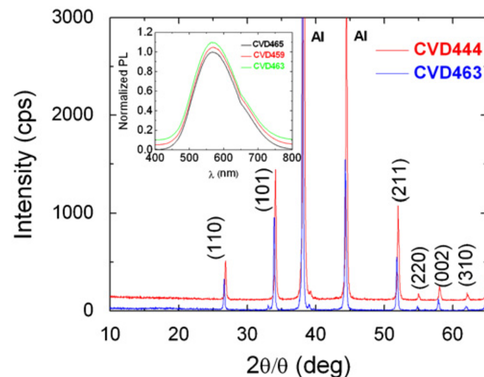

Fig. 2. XRD spectra of the SnO_2 NWs (CVD444) obtained by LPCVD and following post-growth oxidation under 1000 sccm of O_2 at 1000 °C (CVD463). The inset shows the PL spectra of SnO_2 NWs after post-growth oxidation at 400 °C, 700 °C and 1000 °C under 1000 sccm of O_2.

The SnO_2 NWs grown at T_G=800 °C exhibited clear peaks in the XRD spectrum as shown in Fig. 2 corresponding to the (110), (101), (211), (220), (002) and (310) tetragonal rutile structure of SnO_2 [20]. We should point out that the Al peaks appearing in the XRD spectrum of Fig. 2 belong to the sample holder. Also shown in Fig. 2 are the XRD spectra of the SnO_2 NWs following thermal annealing, showing that no significant changes occurred in the crystal structure even at the highest annealing temperatures, i.e. T_A=1000 °C, see Table 1.

In addition there is no change in the RT PL spectra of the SnO_2 NWs after thermal annealing as shown in the inset of Fig. 2 but a reduction in the PL intensity occurred with increasing post-growth oxidation temperature. Previously we had shown that the SnO_2 NWs have a high density of states located in the upper half of the energy band gap close to the conduction-band edge while we also detected the surface plasmon resonance absorption of the Au NPs situated on the ends of the SnO_2 NWs using ultrafast pump-probe spectroscopy [20]. The RT PL spectrum shown in Fig. 2 has a maximum at λ=580 nm and is broad due to radiative recombination of carriers between states that are located energetically in the upper half of the energy band-gap of SnO_2 and the valence band. However upon decreasing the temperature from 100 to 80 K we find that the PL exhibits a blue shift with a maximum at λ=480 nm as shown in Fig. 3, which is due to radiative emission between shallow energy levels located close to the conduction band edge of the SnO_2 NWs and the

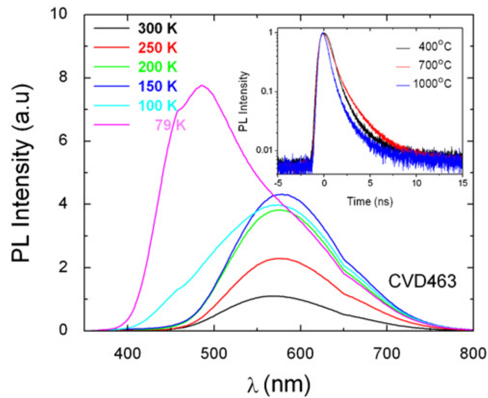

Fig. 3. Temperature dependence of the PL intensity for the SnO_2 NWs treated at 1000 °C under 1000 sccm of O_2. The inset shows RT time resolved-PL intensity of the SnO_2 NWs treated at $T_{OX}=400$ °C, 700 °C and 1000 °C under 1000 sccm of O_2 for 1 h. No significant changes occur in the carrier dynamics.

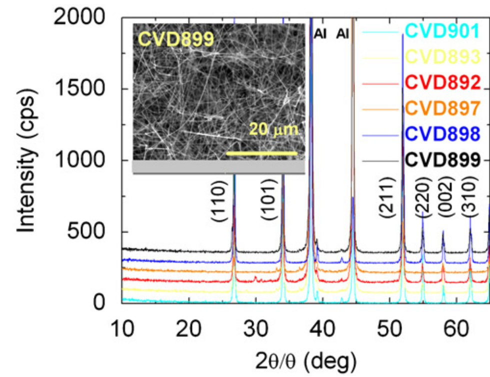

Fig. 5. XRD spectra of SnO_2 NWs treated at $T_N=400$ °C under NH_3:H_2 for 1 h. In bottom-up order the % content of H_2 was 0% lower trace, 10%, 20%, 30%, 40% and 50% top trace and the total flow was kept constant at 200 sccm. The inset shows an SEM image of the SnO_2 NWs after nitridation at 400 °C under NH_3:50% H_2, i.e. CVD899.

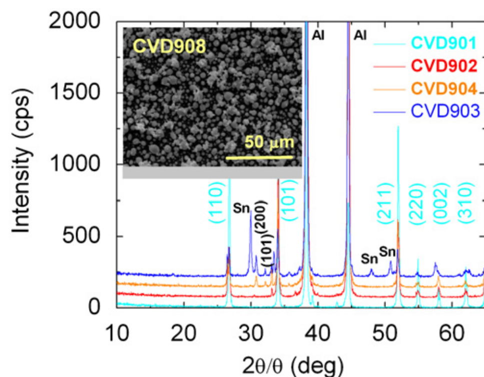

Fig. 4. XRD spectra of SnO_2 NWs treated at various nitridation temperatures, i.e. $T_N=400$ °C (Lower Trace) 500 °C, 510 °C and 520 °C (top trace) under 200 sccm of NH_3 for 1 h. The peaks labeled in bold correspond to Sn, all other to SnO_2. The inset shows an SEM image of the droplets with diameters of 5 μm obtained on Si(001) after nitridation at 600 °C, i.e. CVD908.

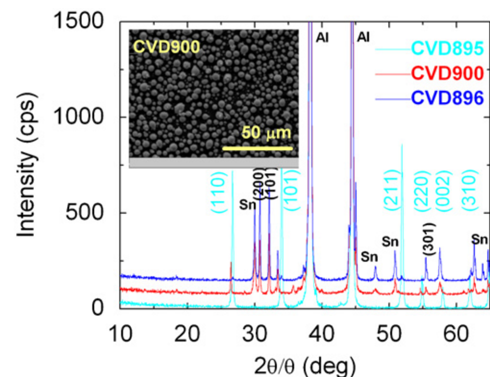

Fig. 6. XRD spectra of SnO_2 NWs treated at $T_N=400$ °C for 1 h and $T_N=500$ °C, 550 °C and 600 °C under 200 sccm of NH_3:20% H_2 for 1 h using a slow ramp rate. The peaks labeled in bold correspond to Sn, all other to SnO_2. The inset shows an SEM image of droplets with diameters of 5 μm obtained on Si(001) after nitridation–hydrogenation at 400 °C and 550 °C, i.e. CVD900.

valence band. The PL at $\lambda=580$ nm is suppressed below 100 K due to filling of the deep-mid-gap states, which allows electrons that are excited close to the conduction band edge to recombine with holes thereby emitting at $\lambda=480$ nm.

In addition we find that thermal annealing has no significant effect on the carrier dynamics as confirmed by time resolved PL shown in the inset of Fig. 3. These findings are consistent with those of Chen et al. [27] who investigated thermal annealing of SnO_2 nanoribbons over a narrower temperature range, i.e. 600–1000 °C and similarly found that the shape of the PL spectra did not change.

In contrast to thermal annealing of SnO_2 NWs, which does not have a significant influence on the structural and optical properties we find that nitridation >500 °C lead to the gradual elimination of the SnO_2 NWs and their conversion into Sn droplets on the surface of the Si(001) as shown in Fig. 4 where a new set of peaks corresponding to the (200) (101) and (301) orientations of Sn have appeared. The remaining peaks correspond to Sn in accordance with other investigations on nanostructured Sn but their crystallographic directions have not been determined [28]. On the other hand we find that the nitridation of the SnO_2 NWs between 400–500 °C is not promoted by the inclusion of H_2 even for H_2 contents up to 50% of the total gas flow as summarized in Table 1. The SnO_2 NWs maintain their integrity and crystal structure as can be clearly seen from the XRD in Fig. 5. No peaks related to Sn make their appearance despite the presence of H_2. Finally we find that employing a two step temperature nitridation process involving NH_3: 20% H_2 and slow ramp rates as listed in Table 1, merely leads to the reduction of the SnO_2 NWs and the formation of Sn, which again clearly show up in the XRD of Fig. 6 similar to that of Fig. 4. The XRD spectrum of the Sn droplets is characterized by clear peaks corresponding to the (200), (101) and (301) orientations of Sn. These findings are in direct contrast with previous investigations on the nitridation of β-Ga_2O_3 or In_2O_3 NWs, which was successfully achieved by employing the nitridation strategies described above [23,24]. The post-growth nitridation of β-Ga_2O_3 and In_2O_3 NWs proceeds via a reduction to Ga_2O and In_2O, respectively, which react with NH_3. Moreover any Ga or In occurring from the reduction will still react with N from thermally dissociated NH_3 giving the corresponding nitride. Now as already seen above we find that the SnO_2 NWs have a preferential tendency to dissociate into Sn under NH_3 while they are remarkably stable at elevated temperatures under O_2. It is very likely therefore that the NH_3 favors the reduction of the SnO_2 into Sn. However, unlike In or Ga, Sn does not react with NH_3 to give Sn_3N_4 since as already explained above Sn_3N_4 NWs were obtained only via the reaction of Sn with HCl and the formation of halides such as $SnCl_2$ and $SnCl_4$ which react readily with NH_3 [18,19].

Therefore we used NH_4Cl in order to promote the conversion of the SnO_2 into Sn_3N_4 NWs via the formation of $SnCl_4$. Initially the SnO_2 NWs were subjected to a flow of 200 sccm of NH_3 between 325 °C and 425 °C using just NH_4Cl, as described in

Table 2. It is well known that NH_4Cl undergoes sublimation at 338 °C according to $NH_4Cl_{(s)} \rightarrow NH_3 + HCl$. We observed the complete elimination of the NH_4Cl at 425 °C, which is consistent with Chaiken et al. [25] who found that the typical sublimation weight loss of NH_4Cl is over 90% when heated for $\approx$60 min at elevated temperatures. A slow ramp rate was employed here to ensure the gradual sublimation of NH_4Cl and the release of HCl, which reacts at the surface of the SnO_2 NWs giving $SnCl_4$, according to $SnO_2 + 4HCl \rightarrow SnCl_4 + 2H_2O$. We observe the suppression of the SnO_2 NWs peaks with increasing temperature i.e 350, 360 and 375 °C shown in Fig. 7, which is attributed to the reaction of SnO_2 with HCl. In this case an excessive 1 g of NH_4Cl was used, which led to the disappearance of the SnO_2 NWs despite the flowing NH_3 and NH_3 released from NH_4Cl. In effect the HCl consumed the SnO_2 NWs, which clearly lead to a suppression in the intensity of the SnO_2 peaks. However it should be noted that we do not find any peaks related to Sn while the post-growth nitridation under NH_3 or NH_3:H_2 without NH_4Cl between 325 °C and 425 °C did not lead to any changes in the structural or optical properties of the SnO_2 NWs corroborating that the HCl reacts with the surface of the SnO_2 NWs giving $SnCl_4$. Upon reducing the amount of NH_4Cl by an order of magnitude and by adding an equal amount of Sn we find that the reaction lead to the formation of tin nitride keeping all other growth conditions identical. This is seen from the small, but nevertheless clearly resolved peaks arising in the XRD spectra of Fig. 7, corresponding to the hexagonal crystal structure of tin nitride in accordance with Lima et al. [14]. No

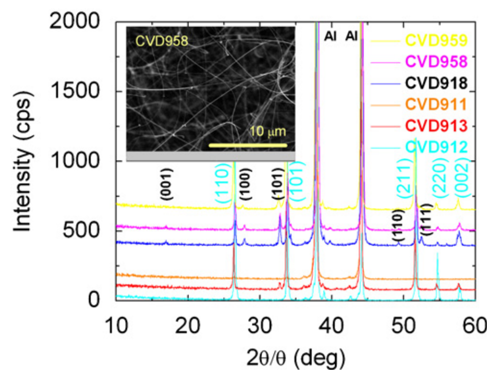

Fig. 7. XRD traces of SnO_2 NWs treated at T_N=400 °C for 1 h under 200 sccm of 20% H_2:NH_3 for 1 h using a ramp rate of 10 °C/min. The peaks labeled on bold correspond to tin nitride, all other to SnO_2. In bottom-up order: (a) using only NH_4Cl at 350 °C, 360 °C and 375 °C, (b) using NH_4Cl:Sn at 425 °C, 450 °C and 475 °C. The inset shows an SEM image of the nanowires after nitridation at 400 °C using NH_4Cl:Sn i.e. CVD958.

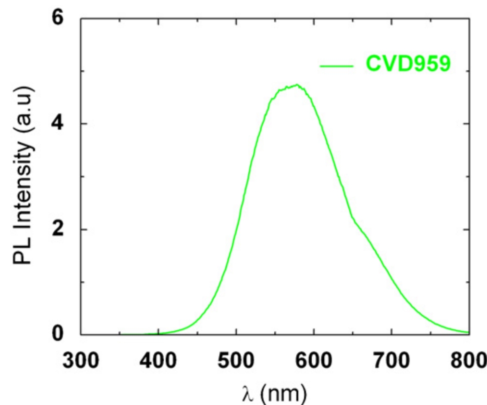

Fig. 8. RT PL spectra from the SnO_2 NWs treated under 0.1 g Sn: 0.1 g NH_4Cl at 475 °C (CVD959).

peaks corresponding to Sn occur as expected. However we still observe peaks related to the SnO_2 NWs in Fig. 7 and we find that the nanowires maintain their integrity as can be seen from the inset in Fig. 7 in contrast to the case of Ga_2O_3 and In_2O_3 NWs where we observed a clear cut suppression of the oxide-related peaks. It is therefore likely that a SnO_2/Sn_3N_4 core–shell structure is created but at the same time we can not rule out the growth of individual Sn_3N_4 NWs in between the SnO_2 NWs. Nevertheless given that the underlying network of interconnected SnO_2 NWs is dense and only a small fraction of the Au/n^+Si(001) surface is exposed to the reacting Sn and NH_4Cl it is more likely that the Sn_3N_4 grows on top of the SnO_2 rather than on Au/n^+Si(001). Last but not the least we find that the post-growth nitridation of the SnO_2 NWs using NH_4Cl:Sn does not lead to a dramatic change in the PL spectrum as shown in Fig. 8. This is consistent with the fact that tin nitride NWs obtained by halide CVD [18,19] exhibited a broad-symmetric PL spectrum centered at 570 nm whose shape did not change between 77 and 300 K [18] and was very similar to that of SnO_2 NWs shown in Fig. 2.

4. Conclusions

SnO_2 NWs with diameters of 50 nm, lengths of several tens of micrometers and a tetragonal rutile crystal structure have been grown at 800 °C on Au/Si(001) via the VLS mechanism and by LPCVD. These exhibited a broad-symmetric PL spectrum but neither the crystal structure nor the optical properties changed by post-growth annealing under a high flow of oxygen between 400 and 1000 °C. In contrast post-growth nitridation using NH_3 at temperatures $>$500 °C lead to the elimination of the SnO_2 NWs but no significant changes occurred in the structural or optical properties at lower temperatures even after including hydrogen or by employing a two-step temperature nitridation process. This is in direct contrast with the nitridation of other metal-oxides such as Ga_2O_3 and In_2O_3 NWs, which were easily converted to GaN and InN, respectively, using the strategies described above and was accompanied by a suppression of the respective oxide phases. The nitridation of SnO_2 NWs was promoted via the reaction of HCl with Sn or SnO_2, supplied in-situ from the sublimation of NH_4Cl, which lead to the formation of $SnCl_4$ that reacted with NH_3 giving tin nitride with a hexagonal crystal structure. In this case the integrity of the nanowires was maintained but the SnO_2 NWs are not completely converted into Sn_3N_4.

References

[1] A. Othonos, M. Zervos, M. Pervolaraki, Nanoscale Research Letters 4 (2009) 122.
[2] D. Tsokkou, A. Othonos, M. Zervos, Journal of Applied Physics 106 (2009) 054311.
[3] T. Kuykendall, P. Ulrich, S. Aloni, P. Yang, Nature Materials 6 (2007) 1961.
[4] H.Y. Kim, J. Park, H. Yang, Chemical Physics Letters 372 (2003) 269.
[5] T. Xie, Z. Jianga, G. Wu, X. Fang, G. Li, L. Zhang, Journal of Crystal Growth 283 (2005) 286.
[6] K.S. Park, Y.J. Park, M.K. Kim, J.T. Son, H.G. Kim, S.J. Kim, Journal of Power Sources 103 (2001) 67.
[7] T. Lindgren, M. Larsson, S.E. Lindquist, Solar Energy Materials 73 (2002) 377.
[8] R.G. Gordon, D.M. Hoffman, U. Riaz, Chemical Materials 4 (1992) 4.
[9] N. Takahashi, K. Terada, T. Nakamura, Journal of Materials Science Letters 20 (2001) 227.
[10] D.M. Hoffman, S.P. Rangarajan, S.D. Athavale, et al., Journal of Vaccum Science and Technology A 13 (1995) 820.
[11] Y. Inoue, M. Nomiya, O. Takai, Vacuum 51 (1998) 673.
[12] R. Kamei, T. Migita, T. Tanaka, K. Kawabata, Vacuum 59 (2000) 764.
[13] L. Maya, Journal of Vaccum Science and Technology A 11 (1993) 604.
[14] R.S. Lima, P.H. Dionisio, W.H. Schreiner, Solid State Communications 79 (1991) 395.
[15] B. Wang, M.J. Callahan, Crystal Growth and Design 6 (2006) 1227.
[16] L. Maya, Inorganic Chemistry 31 (1992) 1958.

[17] S.V. Nand, K. Ankur, K. Brijesh, M.B. Raj, Solid State Sciences 10 (2008) 569.
[18] M. Zervos, A. Othonos, Journal of Crystal Growth 316 (2011) 25.
[19] M. Zervos, A. Othonos, Nanoscale Research Letters 4 (2009) 1103.
[20] A. Othonos, M. Zervos, D. Tsokkou, Nanoscale Research Letters 4 (2009) 828.
[21] A. Othonos, M. Zervos, C. Christofides, Journal of Applied Physics 108 (2010) 124302.
[22] D. Tsokou, M. Zervos, A. Othonos, Journal of Applied Physics 106 (2009) 084307.
[23] A. Othonos, M. Zervos, C. Christofides, Journal of Applied Physics 108 (2010) 124319.
[24] P. Papageorgiou, M. Zervos, A. Othonos, Nanoscale Research Letters 6 (2011) 311.
[25] R.F. Chaiken, D.J. Sibbett, J. Sutherland, et al., Journal of Chemical Physics 37 (1962) 2311.
[26] A. Othonos, M. Zervos, Journal of Applied Physics 106 (2009) 114303.
[27] H.T. Chen, X.L. Wu, S.J. Xiong, W.C. Zhang, J. Zhu, Applied Physics A 97 (2009) 365.
[28] S.S. Chang, D.K. Park, Materials Science and Engineering B95 (2002) 55.